

# Pion Form Factors in Holographic QCD

Herry J. Kwee\* and Richard F. Lebed†

*Department of Physics, Arizona State University, Tempe, AZ 85287-1504*

(Dated: December 2007)

## Abstract

Using a holographic dual model of QCD, we compute the pion electromagnetic form factor  $F_\pi(Q^2)$  in the spacelike momentum transfer region, as well as pion couplings to vector mesons  $g_{\rho^{(n)}\pi\pi}$ . Spontaneous and explicit chiral symmetry breaking are intrinsic features of this particular holographic model. We consider variants with both “hard-wall” and “soft-wall” infrared cutoffs, and find that the  $F_\pi(Q^2)$  data tend to lie closer to the hard-wall model predictions, although both are too shallow for large  $Q^2$ . By allowing the parameters of the soft-wall model (originally fixed by observables such as  $m_\rho$ ) to vary, one finds fits that tend to agree better with  $F_\pi(Q^2)$ . We also compute the pion charge radius  $\langle r_\pi^2 \rangle$  for a variety of parameter choices, and use the values of  $f_\rho^{(n)}$ ,  $g_{\rho^{(n)}\pi\pi}$  and  $m_\rho^{(n)}$  to observe the saturation of  $F_\pi(0)$  by  $\rho$  poles.

PACS numbers: 11.25.Tq, 11.25.Wx, 13.75.Lb

---

\*Electronic address: Herry.Kwee@asu.edu

†Electronic address: Richard.Lebed@asu.edu

## I. INTRODUCTION

Quantum chromodynamics, now in its fourth decade, has been known since its inception to stubbornly resist direct analytical solutions in its strong coupling regime. The modern period has seen numerous approaches developed to tackle this problem, sometimes by providing a simplified picture of strong interactions and its states (e.g., quark potential models, chiral Lagrangians, quenched lattice calculations), or by working in energy or mass regimes where a key parameter may be assumed small (e.g., asymptotic freedom regime calculations, operator-product expansions, heavy quark effective theory), or by studying features of quantum field theories that incorporate distinctly nonperturbative behavior (e.g., solitons, instantons).

Perhaps the most interesting techniques are ones that stimulate advances in studies of QCD-like theories by making them *more* complicated by introducing additional degrees of freedom. In this category one includes the  $1/N_c$  expansion and, more recently, the gravity/gauge correspondence known by the names of the anti-de Sitter/conformal field theory (AdS/CFT) correspondence or the holographic dual approach [1]. This proposed duality between strongly-coupled Yang-Mills theories and weakly-coupled gravity is exceptionally appealing because it implies a fundamental connection between gauge and string theories.

The original example of this duality is given by  $\mathcal{N} = 4$  super-Yang Mills theory, which is conformal and therefore lacks asymptotic  $S$ -matrix particle states. While this hardly seems like an auspicious starting point for modeling QCD-like theories and their rich hadronic spectra, a number of the original dual theories nonetheless possess such useful QCD-like properties as chiral symmetry breaking and confinement. Moreover, approximate conformal symmetry is a well-known property of QCD in the deep ultraviolet (UV) limit.

In the holographic approach one begins with the 5-dimensional AdS metric,

$$ds^2 = g_{MN} dx^M dx^N = \frac{1}{z^2} (\eta_{\mu\nu} dx^\mu dx^\nu - dz^2), \quad (1)$$

where  $\eta_{\mu\nu} = \text{diag}(+, -, -, -)$  is distinguished from the full nontrivial 5D metric  $g_{MN}$  obtained from Eq. (1). The  $z$  (Liouville or “bulk”) coordinate corresponds to an inverse energy scale ( $Q \sim 1/z$ ), in that the UV limit of QCD is represented by fields living on the AdS boundary  $z = 0$  (or, allowing for a UV cutoff, a small finite value  $z = \epsilon$ , a location called the “UV brane”). The gauge/gravity correspondence then states that every CFT operator  $\mathcal{O}(x)$  is

associated with a bulk field  $\Psi(x, z)$  uniquely determined by its value  $\Psi(x, \epsilon)$  on the UV brane. The conformal symmetry is broken, introducing thereby a mass scale, by limiting the ability of the fields  $\Psi(x, z)$  to penetrate deeply into the bulk, which corresponds to constraining the infrared (IR) behavior; this may be accomplished, for example, by imposing a hard cutoff and appropriate boundary conditions on  $\Psi(x, z)$  at a value  $z = z_0$  (called the “IR brane”) [2] or by introducing a soft wall with an exponential decrease  $\sim e^{-\kappa^2 z^2}$  in the action for large  $z$  [3]. The dimensionful parameters  $z_0^{-1}$  or  $\kappa$  consequently serve the role of  $\Lambda_{\text{QCD}}$ . The Kaluza-Klein modes of the field  $\Psi(x, z)$  then represent hadronic states of the same quantum numbers, producing towers of hadrons analogous to those arising in the original hadronic flux-tube string theories of the 1970’s, which in turn are in close kinship with the original Regge theories of hadronic excitations.

Fully exploiting the gauge/gravity correspondence to produce a model for real strong interaction physics—a method called “holographic QCD” or “AdS/QCD”—may be attempted either through a top-down approach starting with a particular string theory and choosing a background that (as mentioned above) naturally produces QCD-like properties, or a bottom-up approach starting with real QCD properties and using them to obtain constraints on viable dual gravity theories. In this paper we adopt the latter viewpoint. Work along these lines has become very popular in the past couple of years; especially well represented and close to this work in spirit are studies of hadronic spectra [3, 4, 5, 6, 7, 8, 9, 10], the couplings of hadrons in the presence of chiral symmetry breaking [4, 11, 12, 13, 14], and hadronic form factors [15, 16, 17, 18, 19]. In this paper we are specifically interested in employing the formalism introduced in Ref. [4], in which chiral symmetry breaking is included directly in the Lagrangian, to obtain specific information on the form factor of the pion in this variant of AdS/QCD.

According to the holographic correspondence, the global QCD symmetry of isospin associated with the two light quark flavors is promoted to a gauged  $SU(2)$  symmetry respected by the bulk fields, and the problem reduces to one of constructing a 5D action containing all the fields of interest with the appropriate quantum numbers and Lorentz structures. Varying the action with respect to the fields of interest generates their wave equations, which are solved as eigenvalue equations subject to appropriate boundary conditions to obtain the modes (mesons with particular masses and  $z$ -dependent wave functions). Meson decay constants appear as values of the modes at the UV boundary (associated, as usual, with wave

functions at small distance scales) and form factors appear as convolution integrals over  $z$  of wave functions and currents.

The behavior of wave functions and form factors of vector mesons (the  $\rho$  and its partners) has been examined using the constructions of Ref. [4] using both hard-wall [15] and soft-wall [16] IR boundary conditions. The former has the advantage of simplicity but produces the unphysical Regge trajectory  $M_n^2 \sim n^2$ , while the latter produces the more phenomenologically realistic behavior  $M_n^2 \sim n^1$  [3]. A number of interesting results follow from the analysis of Refs. [15, 16], including a distinctive pattern of vector meson dominance by the lowest-mass states and predictions of the  $\rho$  charge radius. However, the calculations of Refs. [15, 16] require only one dimensionful parameter,  $z_0$  or  $\kappa$ , respectively, and their eigenvalue equations for the vector mesons admit closed-form analytic solutions in terms of known functions (Bessel functions and Laguerre polynomials). The pion sector as described in Ref. [4] also requires dimensionful parameters associated with both spontaneous ( $\sigma$ ) and explicit ( $m_q$ ) chiral symmetry breaking, and the resultant wave equations cannot be solved in closed form for arbitrary values of the three dimensionful parameters. It is the purpose of this paper to examine both the analytic limiting cases of the pion interpolating field and numerical solutions for pion couplings and form factor, in both the hard- and soft-wall cases.

In our numerical simulations we find that the data for the pion form factor  $F_\pi(Q^2)$  lies closer to the hard-wall than the soft-wall model results. The three parameters of the hard-wall model were originally fit to  $m_\rho$ ,  $m_\pi$ , and  $f_\pi$ , and we repeat the exercise for the parameters of the corresponding soft-wall model. One may adjust the parameters of either model to obtain a better fit to  $F_\pi(Q^2)$ , but at the cost of a poorer fit to at least one of these three observables. The  $F_\pi(Q^2)$  data suggests an optimal model that incorporates features of both, but is closer to the hard-wall model.

A calculation [20] using the same formalism of Ref. [4] considers  $F_\pi(Q^2)$  in the chiral limit (*i.e.*, sets  $m_q = 0$ ) and focuses primarily on analytical behavior. We agree with their finding that the original hard-wall model overshoots  $F_\pi(Q^2)$  data for large  $Q^2$  (but not with their choice of normalization for parameters such as  $f_\pi$ ).

This paper is organized as follows: In Sec. II we recount and extend the formalism of Ref. [4] relevant to our calculations and exhibit the analytically soluble limits to the equations of motion for the field containing the pion modes. Section III gives expressions for the pion form factor and couplings in terms of AdS/QCD mode wave functions. Section IV presents

the results of a number of numerical simulations of the pion electromagnetic form factor and couplings to vector mesons, and Sec. V summarizes our results and concludes.

## II. FORMALISM

The full 5-dimensional action [4] used in this work reads

$$S = \int d^5x e^{-\Phi} \sqrt{g} \operatorname{Tr} \left\{ |DX|^2 + 3|X|^2 - \frac{1}{4g_5^2} (F_L^2 + F_R^2) \right\}, \quad (2)$$

where  $g \equiv |\det g_{MN}|$  is obtained from the metric in Eq. (1), and  $e^{-\Phi}$  represents a background dilaton coupling, with  $\Phi(z) = 0$  in the hard-wall case and  $\kappa^2 z^2$  in the soft-wall case. The Lagrangian within the braces of Eq. (2) is written in terms of a scalar field  $X$  and chiral gauge fields  $A_{L,R}$  that enter through  $D^M X \equiv \partial^M X - iA_L^M X + iX A_R^M$ ,  $A_{L,R}^M \equiv A_{L,R}^{M a} t^a$  with  $t^a$  being the generators of the gauged isospin symmetry, and  $F_{L,R}^{MN} \equiv \partial^M A_{L,R}^N - \partial^N A_{L,R}^M - i[A_{L,R}^M, A_{L,R}^N]$ . The chiral gauge fields  $A_{L,R}^{M a}$  are the holographic partners of the QCD operators  $\bar{q}_{L,R} \gamma^\mu t^a q_{L,R}$ , while  $X^{\alpha\beta}$  [more precisely  $(2/z)X^{\alpha\beta}$ ] is associated with  $\bar{q}_R^\alpha q_L^\beta$ , and therefore incorporates all chiral symmetry-breaking behavior. In the holographic dictionary of Ref. [4], the vacuum expectation value  $X_0$  of  $X$  (exact for the hard-wall model) is given by

$$X_0(z) = \frac{1}{2} M z + \frac{1}{2} \Sigma z^3, \quad (3)$$

where  $M = m_q \mathbb{1}$  and  $\Sigma = \sigma \mathbb{1}$  represent explicit and spontaneous chiral symmetry breaking, respectively, and arise in the holographic recipe through the normalizable and nonnormalizable solutions for the bulk field  $X$ . Strictly speaking, Eq. (3) holds for the soft-wall model only for small values of  $z$  [3]; for large  $z$  the corresponding  $X_0$  should approach a constant, but the  $e^{-\kappa^2 z^2}$  background minimizes this distinction. We perform subsequent calculations using a background field that formally satisfies both limiting forms in Ref. [21]; however, as shown there, the best fits do not improve upon the naive soft-wall fits presented below. The pion field  $\pi^a$  appearing through  $X = X_0 \exp(2i\pi^a t^a)$  is dimensionless and related to the canonically-normalized pion field  $\tilde{\pi}^a$  of chiral Lagrangians via  $\pi^a = \tilde{\pi}^a / f_\pi$ , with  $f_\pi = 93$  MeV.

One now forms the polar and axial gauge fields  $V, A$ :  $V^M \equiv \frac{1}{2}(A_L^M + A_R^M)$  and  $A^M \equiv \frac{1}{2}(A_L^M - A_R^M)$ , in terms of which  $D^M X = \partial^M X - i[V^M, X] - i\{A^M, X\}$ ,  $F_V^{MN} \equiv \partial^M V^N - \partial^N V^M - i([V^M, V^N] + [A^M, A^N])$ ,  $F_A^{MN} \equiv \partial^M A^N - \partial^N A^M - i([V^M, A^N] + [A^M, V^N])$ , and

$$S = \int d^5x e^{-\Phi} \sqrt{g} \operatorname{Tr} \left\{ |DX|^2 + 3|X|^2 - \frac{1}{2g_5^2} (F_V^2 + F_A^2) \right\}. \quad (4)$$

This action represents the only terms quadratic in fields and containing two derivatives or less, and is therefore sufficient to obtain the free-field equations of motion for  $V_M$ ,  $A_M$ , and  $\pi$  [generically  $\Psi(x, z)$ ]. It is convenient to work in an axial-like gauge,  $V_z(x, z) = 0$ ,  $A_z(x, z) = 0$ ; the associated sources may then be expressed as divergences over only the usual four spacetime dimensions,  $\partial^\mu V_\mu = 0$  (since isospin is conserved) and  $\partial^\mu A_\mu$ .  $A_\mu$  is further decomposed into a transverse (divergenceless) piece  $A_{\mu\perp}$  and a longitudinal piece  $\varphi$ :  $A_\mu = A_{\mu\perp} + \partial_\mu \varphi$ . The fields are chosen to satisfy Neumann conditions  $\partial_z \Psi(x, z) = 0$  at  $z = z_0$  in the hard-wall case and to give a vanishing contribution from the  $z \rightarrow \infty$  limit in the soft-wall case.

Solving for the equations of motion of the fields  $\Psi(q, z)$  Fourier transformed with respect to the 4D coordinates  $x$  yields

$$\partial_z \left( \frac{e^{-\Phi}}{z} \partial_z V_\mu^a \right) + \frac{q^2 e^{-\Phi}}{z} V_\mu^a = 0, \quad (5)$$

$$\left[ \partial_z \left( \frac{e^{-\Phi}}{z} \partial_z A_\mu^a \right) + \frac{q^2 e^{-\Phi}}{z} A_\mu^a - \frac{g_5^2 v(z)^2 e^{-\Phi}}{z^3} A_\mu^a \right]_\perp = 0, \quad (6)$$

$$\partial_z \left( \frac{e^{-\Phi}}{z} \partial_z \varphi^a \right) + \frac{g_5^2 v(z)^2 e^{-\Phi}}{z^3} (\pi^a - \varphi^a) = 0, \quad (7)$$

$$-q^2 \partial_z \varphi^a + \frac{g_5^2 v(z)^2}{z^2} \partial_z \pi^a = 0, \quad (8)$$

where  $v(z) = 2X_0(z) = m_q z + \sigma z^3$ . Whereas Refs. [15, 16] obtain solutions of Eq. (5) (corresponding to the tower of  $\rho$  states), we focus instead on Eqs. (7) and (8), coupled equations corresponding to the  $\pi$  and its excitations. The dimensionful chiral symmetry-breaking parameters  $m_q$  and  $\sigma$  render Eqs. (7) and (8) [as well as Eq. (6)] more complicated than Eq. (5), which depends upon only one dimensionful parameter,  $z_0$  or  $\kappa$ .

The gauge/gravity correspondence provides a method of determining the 5D gauge coupling  $g_5$ . Applying the equation of motion Eq. (5) to the  $F_V^2$  portion of the action Eq. (4) leaves only the boundary term

$$S = -\frac{1}{2g_5^2} \int d^4x \left. \frac{e^{-\Phi}}{z} V_\mu^a \partial_z V^{\mu a} \right|_{z=\epsilon}. \quad (9)$$

The significance of this quantity becomes clear when one resolves the vector field as  $V_\mu^a(q, z) = V(q, z) \tilde{V}_\mu^a(q)$ , where  $\tilde{V}_\mu^a(q)$  is the Fourier transform of the source of the vector current  $J_\mu^a = \bar{q} \gamma_\mu t^a q$  at the UV boundary  $z = \epsilon$ , and  $V(q, z)$  (the “bulk-to-boundary propagator”) is normalized to  $V(q, \epsilon) = 1$ . Due to the isospin conservation constraint  $q_\mu V^\mu = 0$ , one

may replace  $\tilde{V}_\mu^a \tilde{V}^{\mu a}$  with  $\tilde{V}_\mu^a \tilde{V}_\nu^b \Pi^{\mu\nu} \delta^{ab}$  and  $\Pi^{\mu\nu} \equiv \eta^{\mu\nu} - q^\mu q^\nu / q^2$ , and then the usual quadratic variation of the action with respect to the source  $\tilde{V}$  produces the vector current two-point function:

$$\int d^4x e^{iqx} \langle J_\mu^a(x) J_\nu^b(0) \rangle = \delta^{ab} \Pi_{\mu\nu} \Sigma_V(q^2), \quad (10)$$

$$\Sigma_V(q^2) = - \frac{e^{-\Phi}}{g_5^2} \frac{\partial_z V(q, z)}{z} \Big|_{z=\epsilon}, \quad (11)$$

from which one finds, matching to the QCD result for currents  $J_\mu$  normalized [16] according to the prescription of [4]

$$g_5^2 = \frac{12\pi^2}{N_c} \rightarrow 4\pi^2. \quad (12)$$

An analogous calculation in the axial sector relates the bulk-to-boundary propagator  $A(q, z)$  to the  $\pi$  decay constant  $f_\pi$ :

$$f_\pi^2 = - \frac{1}{g_5^2} \frac{\partial_z A(0, z)}{z} \Big|_{z=\epsilon}. \quad (13)$$

The sets of normalizable eigenstates of Eqs. (5)–(8) form towers of hadrons of the corresponding quantum numbers. Since large  $N_c$  is intrinsic to this procedure, the mesons have narrow widths and the spectral decompositions of self-energy functions such as  $\Sigma_V$  are sums over poles:

$$\Sigma_V(q^2) = \sum_{n=0}^{\infty} \frac{f_n^2}{q^2 - M_n^2}, \quad (14)$$

where  $M_n$  are the mass eigenvalues and  $f_n$  are the decay constants of vector modes  $\psi_n(z)$  normalized according to

$$\int dz \frac{e^{-\Phi}}{z} \psi_m(z) \psi_n(z) = \delta_{mn}. \quad (15)$$

The coupled equations of motion Eqs. (7)–(8) for the bulk-to-boundary propagators  $\partial_z \varphi(q, z)$ ,  $\partial_z \pi(q, z)$  can be combined to produce the decoupled and dimensionless Sturm-Liouville form

$$\partial_x [\Lambda(x) \partial_x y(x)] + \Lambda(x) [\tilde{q}^2 - \beta(x)] y(x) = 0, \quad (16)$$

where, taking  $\mu \equiv 1/z_0$  or  $\kappa$  in the hard- and soft-wall cases, respectively, the dimensionless independent and dependent variables are  $x \equiv \mu z$  and  $y(x) \equiv [e^{-\Phi(x/\mu)} / x] [\partial_x \varphi(\mu \tilde{q}, x/\mu)]$ , respectively. Furthermore,  $\tilde{q}^2 \equiv q^2 / \mu^2$  and  $\beta(x) \equiv g_5^2 v(\mu x)^2 / x^2$ , or

$$\beta(x) \equiv (\tilde{m}_q + \tilde{\sigma} x^2)^2, \quad (17)$$

where  $\tilde{m}_q \equiv g_5 m_q / \mu$  and  $\tilde{\sigma} \equiv g_5 \sigma / \mu^3$  are dimensionless, and  $\Lambda(x) \equiv x / [\beta(x) e^{-\Phi(x/\mu)}]$ . Equation (8) then immediately gives a solution for the field  $\partial_z \pi(q, z)$ :

$$\partial_x \pi(\mu \tilde{q}, x/\mu) = \tilde{q}^2 \Lambda(x) y(x). \quad (18)$$

Equation (16) is therefore a second-order ordinary differential equation in  $x$  with three dimensionless parameters,  $\tilde{q}^2$ ,  $\tilde{m}_q$ , and  $\tilde{\sigma}$ . It appears not to admit a general closed-form solution in terms of well-known functions. However, one may, as in this paper, numerically solve the equation subject to physical constraints (fitting to  $m_\rho$ ,  $f_\pi$ , and  $m_\pi$ ). One may also explore limiting cases for various orderings of the parameters; since  $\tilde{\sigma}$  enters Eq. (16) through the combination  $\tilde{\sigma} x^2$ , one may consider the behavior of (16) in the limits where various ratios of  $\tilde{q}^2$ ,  $(\tilde{\sigma} x^2)^2$ , and  $\tilde{m}_q^2$  are taken to be small.

In the hard-wall case of  $\Phi(x/\mu) = 1$ , the analytically soluble cases are

**1)**  $\tilde{q}^2, \tilde{m}_q^2 \gg (\tilde{\sigma} x^2)^2$  ( $z$  small or  $\sigma = 0$ ) :

$$\begin{aligned} y(x) &= A J_0 \left( \sqrt{\tilde{q}^2 - \tilde{m}_q^2} x \right) + B Y_0 \left( \sqrt{\tilde{q}^2 - \tilde{m}_q^2} x \right), \text{ or} \\ \partial_z \varphi(q, z) &= \frac{z}{z_0^2} \left[ A J_0 \left( \sqrt{q^2 - g_5^2 m_q^2} z \right) + B Y_0 \left( \sqrt{q^2 - g_5^2 m_q^2} z \right) \right], \\ \partial_z \pi(q, z) &= \frac{q^2 z}{g_5^2 m_q^2 z_0^2} \left[ A J_0 \left( \sqrt{q^2 - g_5^2 m_q^2} z \right) + B Y_0 \left( \sqrt{q^2 - g_5^2 m_q^2} z \right) \right]. \end{aligned} \quad (19)$$

For extremely small or negative  $q^2$  (such that the arguments of the square roots become negative), the Bessel functions  $J_0$  and  $Y_0$  of course analytically continue to modified Bessel functions.

**2)**  $\tilde{q}^2 \gg (\tilde{\sigma} x^2)^2 \gg \tilde{m}_q^2$  ( $q^2$  large,  $z$  not extremely small) :

$$\begin{aligned} y(x) &= x^2 [A J_2(\tilde{q} x) + B Y_2(\tilde{q} x)], \text{ or} \\ \partial_z \varphi(q, z) &= \frac{z^3}{z_0^4} [A J_2(q z) + B Y_2(q z)], \\ \partial_z \pi(q, z) &= \frac{q^2}{g_5^2 \sigma^2 z z_0^4} [A J_2(q z) + B Y_2(q z)]. \end{aligned} \quad (20)$$

The distinction between **1)** and **2)** arises from a noncommutativity of limits in  $\Lambda(x)$ : If  $\tilde{\sigma} x^2$  is taken small first, then  $\Lambda(x) \rightarrow x / \tilde{m}_q^2$ , while if  $\tilde{m}_q^2$  is taken small first, then  $\Lambda(x) \rightarrow 1 / \tilde{\sigma}^2 x^3$ .



3)  $(\tilde{\sigma}x^2)^2 \gg \tilde{q}^2 \gg \tilde{m}_q^2$  ( $z$  large) :

$$\begin{aligned}
y(x) &= A \text{Ai}' \left[ \left( \frac{\tilde{\sigma}x^3}{2} \right)^{2/3} \right] + B \text{Bi}' \left[ \left( \frac{\tilde{\sigma}x^3}{2} \right)^{2/3} \right], \text{ or} \\
\partial_z \varphi(q, z) &= \frac{z}{z_0^2} \left\{ A \text{Ai}' \left[ \left( \frac{g_5 \sigma z^3}{2} \right)^{2/3} \right] + B \text{Bi}' \left[ \left( \frac{g_5 \sigma z^3}{2} \right)^{2/3} \right] \right\}, \\
\partial_z \pi(q, z) &= \frac{q^2}{g_5^2 \sigma^2 z^3 z_0^2} \left\{ A \text{Ai}' \left[ \left( \frac{g_5 \sigma z^3}{2} \right)^{2/3} \right] + B \text{Bi}' \left[ \left( \frac{g_5 \sigma z^3}{2} \right)^{2/3} \right] \right\}. \quad (21)
\end{aligned}$$

Note that all the special functions appearing in this case are variants of Bessel functions, as seen repeatedly in previous papers that consider solutions to Eq. (5) for the hard-wall background.

In the soft-wall case of  $\Phi(x/\mu) = x^2$ , the only analytically soluble cases turn out to have large  $q^2$ , and the functions are variants on Kummer functions  $M(a, b, z)$ ,  $U(a, b, z)$  (or equivalently, confluent hypergeometric or Whittaker functions) [22]; similar functions have been seen for solutions to Eq. (5) for the soft-wall background [16]. The analytically soluble cases are

1)  $\tilde{q}^2, \tilde{m}_q^2 \gg (\tilde{\sigma}x^2)^2$  ( $z$  small or  $\sigma=0$ ) :

$$\begin{aligned}
y(x) &= e^{-x^2} \left\{ A M \left[ 1 - \frac{1}{4}(\tilde{q}^2 - \tilde{m}_q^2), 1, x^2 \right] + B U \left[ 1 - \frac{1}{4}(\tilde{q}^2 - \tilde{m}_q^2), 1, x^2 \right] \right\}, \text{ or} \\
\partial_z \varphi(q, z) &= \kappa^2 z \left\{ A M \left[ 1 - \frac{q^2 - g_5^2 m_q^2}{4\kappa^2}, 1, (\kappa z)^2 \right] + B U \left[ 1 - \frac{q^2 - g_5^2 m_q^2}{4\kappa^2}, 1, (\kappa z)^2 \right] \right\}, \\
\partial_z \pi(q, z) &= \frac{q^2 \kappa^2 z}{g_5^2 m_q^2} \left\{ A M \left[ 1 - \frac{q^2 - g_5^2 m_q^2}{4\kappa^2}, 1, (\kappa z)^2 \right] + B U \left[ 1 - \frac{q^2 - g_5^2 m_q^2}{4\kappa^2}, 1, (\kappa z)^2 \right] \right\}. \quad (22)
\end{aligned}$$

2)  $\tilde{q}^2 \gg (\tilde{\sigma}x^2)^2 \gg \tilde{m}_q^2$  ( $q^2$  large,  $z$  not extremely small) :

$$\begin{aligned}
y(x) &= x^4 e^{-x^2} \left[ A M(1 - \tilde{q}^2/4, 3, x^2) + B U(1 - \tilde{q}^2/4, 3, x^2) \right], \text{ or} \\
\partial_z \varphi(q, z) &= \kappa^6 z^5 \left\{ A M[1 - q^2/4\kappa^2, 3, (\kappa z)^2] + B U[1 - q^2/4\kappa^2, 3, (\kappa z)^2] \right\}, \\
\partial_z \pi(q, z) &= \frac{q^2 \kappa^6 z}{g_5^2 \sigma^2} \left\{ A M[1 - q^2/4\kappa^2, 3, (\kappa z)^2] + B U[1 - q^2/4\kappa^2, 3, (\kappa z)^2] \right\}. \quad (23)
\end{aligned}$$

Numerous well-known recursion relations, distinct in form for  $M$  and  $U$ , may be used to reduce the arguments of the Kummer functions [22], but we opt to present expressions for which  $M$  and  $U$  have the same arguments.

### III. FORM FACTOR EXPRESSIONS

In the present calculations we are interested in the behavior of both form factors and the 3-point couplings  $g_{n\pi\pi}$  [or  $g_{\rho^{(n)}\pi\pi}$ ] between the  $n$ th vector state and the lowest eigenstate of the field  $\pi$ . Of course, the  $n=0$  case is the AdS/QCD version of  $g_{\rho\pi\pi}$ . In order to identify these couplings, one must expand the action Eq. (4) to cubic order in fields. Since Eq. (8) relates the pion field to the longitudinal mode  $\partial^\mu\varphi$  of  $A^\mu$ , one must identify not only  $V\pi\pi$  terms, but also  $VAA$  and  $VA\pi$ . Schematically,  $DX \sim \partial\pi + \pi\partial\pi + O(\pi^3) + V\pi + O(V\pi^3) + A + A\pi + O(A\pi^2)$ ,  $F_V \sim \partial V + VV + AA$ , and  $F_A \sim \partial A + VA$ .  $X$ , the only field carrying SU(2) fundamental representation indices, must appear at least in pairs, while the  $\partial A$  term of  $F_A$  contains no longitudinal piece:  $\partial^\mu(\partial^\nu\varphi) - \partial^\nu(\partial^\mu\varphi) = 0$ . The relevant terms then arise from the cross terms  $(\partial\pi)(V\pi)$  and  $(V\pi)(A)$  of  $|DX|^2$  and  $(\partial V)(AA)$  of  $F_V^2$ . One obtains the  $V\pi\pi$  terms

$$S_{\text{AdS}}^{V\pi\pi} = \epsilon_{abc} \int d^4x \int dz e^{-\Phi} \left[ \frac{1}{g_5^2 z} (\partial_z \partial^\mu \varphi^a) V_\mu^b (\partial_z \varphi^c) + \frac{v(z)^2}{z^3} (\partial^\mu \pi^a - \partial^\mu \varphi^a) V_\mu^b (\pi^c - \varphi^c) \right]. \quad (24)$$

where the integration ranges over  $[0, z_0]$  in the hard-wall case and  $[0, \infty)$  in the soft-wall case [23]. Reference [4] uses this action (not including the dilaton coupling) to obtain the  $V\pi\pi$  couplings [Eq. (33) below], with the caveat that terms cubic in  $F_{V,A}$  have not been included. In fact, we now show that no such terms contribute to the  $V\pi\pi$  coupling.

The field strength tensors  $F_{V,A}^{MN}$  are antisymmetric and of opposite parities. Due to antisymmetry, only one  $F_V^3$  term ( $\equiv F_V^L{}_M F_V^M{}_N F_V^N{}_L$ ) and one  $F_V F_A^2$  term occurs, while the terms with an odd number of  $F_A$ 's are pseudoscalars. It is tempting to remove the parity distinction by forming the dual  $\mathcal{F}_A$  of  $F_A$ , but in 5D this object is a rank-3 tensor:

$$\mathcal{F}_{JKL} \equiv \frac{1}{6} \epsilon_{JKLMN} F^{MN}. \quad (25)$$

Pairs of Levi-Civita tensors may always be converted into metric tensors using (5D versions of) the usual identities, so the only additional terms one might consider have a single  $\mathcal{F}_A$ . But such terms cannot form scalars because they have an odd total number of Lorentz indices. Thus, only  $F_V^3$  and  $F_V F_A^2$  need be considered.

However,  $F_V^3$  terms that are linear in  $V$  contain at least 5  $\pi$ 's, while the surviving terms of  $F_A$  contain at least one  $V$ , and therefore all terms in  $F_V F_A^2$  are at least quadratic in  $V$ . It follows that none of the  $F^3$  terms contribute to the  $V\pi\pi$  coupling.

Returning to the action Eq. (24), a naive variation gives the 3-point correlator:

$$\langle J_\pi^a(p_1) J_V^{\mu,b}(q) J_\pi^c(-p_2) \rangle = \epsilon^{abc} F(p_1^2, p_2^2, q^2) (p_1 + p_2)^\mu i(2\pi)^4 \delta^{(4)}(p_1 - p_2 + q) . \quad (26)$$

Again recalling the narrowness of resonances, one may express the dynamical factor  $F(p_1^2, p_2^2, q^2)$  in terms of transition form factors:

$$F(p_1^2, p_2^2, q^2) = \sum_{n,k=1}^{\infty} \frac{f_n f_k F_{nk}(q^2)}{(p_1^2 - M_n^2)(p_2^2 - M_k^2)} , \quad (27)$$

where  $F_{nk}(q^2)$  correspond to form factors for  $n \rightarrow k$  transitions. The pion form factor  $F_\pi(q^2)$  is then obtained as

$$F_\pi(q^2) \equiv F_{11}(q^2) = \int dz e^{-\Phi} \frac{V(q, z)}{f_\pi^2} \left\{ \frac{1}{g_5^2 z} [\partial_z \varphi(z)]^2 + \frac{v(z)^2}{z^3} [\pi(z) - \varphi(z)]^2 \right\} , \quad (28)$$

an expression whose origin may be recognized in Eq. (24). It is directly derived from that equation by factoring the 5D fields into products of the (dimensionless) 4D pion fields  $\pi^a(q)$  and the bulk-to-boundary propagators  $\pi(z)$  and  $\varphi(z)$ . In order for the  $\pi^a(q)$  kinetic energy term to receive the standard canonical normalization  $\frac{1}{2} \partial_\mu \pi^a \partial^\mu \pi^a$ , the integral in Eq. (24) [at  $q^2 = 0$ , where  $V(q, z) = 1$ ] must equal unity, which fixes the normalization of Eq. (24). Note that the explicit  $f_\pi^2$  factor in Eq. (24) is part of the normalization and does not change the shape of  $F_\pi(Q^2)$ . The pion is the ground-state solution to Eqs. (7)–(8) subject to the constraints at the large- $z$  termini described in Sec. II. The integral in Eq. (28), setting  $V(q, z) = 1$ , is normalized to unity, giving a canonically-normalized kinetic energy term for the 4D pion field. Taking a spacelike momentum transfer  $q^2 \equiv -Q^2$  for the vector source  $V$  that solves Eq. (5) gives [15]

$$V(q, z) \equiv \mathcal{J}(Q, z) = Qz \left[ K_1(Qz) + I_1(Qz) \frac{K_0(Qz_0)}{I_0(Qz_0)} \right] , \quad (29)$$

for the hard-wall case, while the corresponding expression for the soft-wall case is [16, 19]

$$V(q, z) \equiv \mathcal{J}(Q, z) = \Gamma(1 + Q^2/4\kappa^2) U[Q^2/4\kappa^2, 0, (\kappa z)^2] . \quad (30)$$

Both of these solutions satisfy the boundary conditions  $V(q, \epsilon) = 1$ ,  $V(0, z) = 1$ , as well as  $\partial_z V(q, z) = 0$  for  $z = z_0$  in the hard-wall case. In addition, for large  $z$  Eq. (30) falls as  $(z^2)^{-Q^2/4}$ . Expressing instead  $V(q, z)$  for timelike momentum transfers gives

$$V(q, z) = -g_5 \sum_{n=1}^{\infty} \frac{f_n \psi_n(z)}{q^2 - M_n^2} . \quad (31)$$

Substituting this expression into Eq. (28), one can represent the timelike pion form factor as a sum over vector meson poles:

$$F_\pi(q^2) = - \sum_{n=1}^{\infty} \frac{f_n g_{n\pi\pi}}{q^2 - M_n^2}, \quad (32)$$

where  $g_{n\pi\pi}$  is given by

$$g_{n\pi\pi} = \frac{g_5}{f_\pi^2} \int dz \psi_n(z) e^{-\Phi} \left\{ \frac{1}{g_5^2 z} [\partial_z \varphi(z)]^2 + \frac{v(z)^2}{z^3} [\pi(z) - \varphi(z)]^2 \right\}. \quad (33)$$

Together, Eqs. (28) with Eqs. (29) or (30) and Eqs. (32)–(33) provide a complete expression for the pion form factor in all kinematic regions.

#### IV. RESULTS

In this section we present numerical predictions for QCD observables in both the hard- and soft-wall models. We perform the fit for the three hard-wall parameters  $z_0$  ( $z_m$  in [4]),  $m_q$ , and  $\sigma$  to the three observables  $m_\rho$ ,  $m_\pi$ , and  $f_\pi$ . To the same observables we also fit the three parameters  $\kappa$ ,  $m_q$ , and  $\sigma$  of the soft-wall model. In the hard-wall case the  $\rho$  wave functions [eigenfunctions of Eq. (5)] are Bessel functions, with masses determined by zeroes of  $J_0(qz_0)$ ; hence,  $m_\rho = \gamma_{0,1}/z_0 = 775.5$  MeV, where  $\gamma_{0,1} = 2.405$  fixes  $z_0 = 1/(322$  MeV). One may then fit  $m_q$  and  $\sigma$  to the experimental values of  $m_\pi$  and  $f_\pi$  [which are constrained by the Gell-Mann–Oakes–Renner (GMOR) relation  $m_\pi^2 f_\pi^2 = 2m_q \sigma$ ], yielding  $m_q = 2.30$  MeV and  $\sigma = (326$  MeV)<sup>3</sup> for the hard-wall model. In the soft-wall model the vector mass eigenvalues grow linearly in  $n$  [ $m_{\rho,n}^2 = 4(n+1)\kappa^2$ ]; hence, the  $\rho$  ( $n=0$ ) mass fixes  $\kappa = m_\rho/2 = 389$  MeV. Note in particular that  $m_\rho$  is fixed entirely by the value of  $\mu = 1/z_0$  or  $\kappa$ ;  $m_q$  and  $\sigma$  can then be fit to the experimental values of  $m_\pi$  and  $f_\pi$ , yielding for the soft-wall model  $m_q = 1.45$  MeV and  $\sigma = (368$  MeV)<sup>3</sup>.

Predictions for other QCD observables in both models are collected in Table I. Already one sees that the soft-wall model predicts  $f_\rho$  to be much smaller than the experimental data, while the hard-wall model predicts a much closer value. Indeed, as noted in Ref. [16], the soft-wall model predicts the ratio  $m_\rho^2/f_\rho$  to be exactly  $2\sqrt{2}\pi = 8.89$ , which differs dramatically from the experimental value  $5.02 \pm 0.04$  obtained from Table I; in comparison, the hard-wall model predicts this ratio to be  $\sqrt{2}\pi\gamma_{0,1}J_1(\gamma_{0,1}) = 5.55$ .

In Figs. 1 and 2 we plot the electromagnetic pion form factor  $F_\pi(Q^2)$  in the spacelike region as obtained from both models. While results for both models are too shallow for all

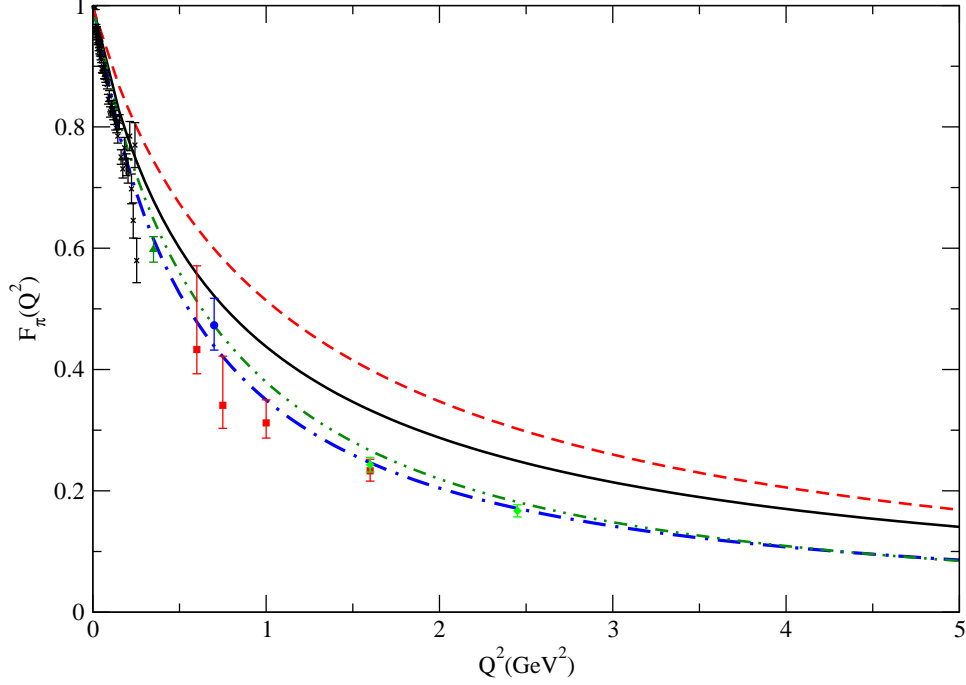


FIG. 1: Spacelike scaling behavior of  $F_\pi(Q^2)$  as a function of  $Q^2 = -q^2$ . The continuous line is the prediction of the original hard-wall model. The dashed line is the prediction of the original soft-wall model with  $\kappa = m_\rho/2$ . The dash-dot line is the hard-wall model with  $\sigma = (254 \text{ MeV})^3$ , and the dash-double-dot line is the soft-wall model with  $\sigma = (262 \text{ MeV})^3$ . The crosses are from a data compilation from CERN [28], the circles are from DESY, reanalyzed by Tadevosyan *et al.* [29, 31], the triangle is data from DESY [30], and the boxes [31] and diamonds [32] are from Jefferson Lab. Older data in the range 3–10  $\text{GeV}^2$  [33] exist but have large uncertainties and are not plotted here.

$Q^2$ , the hard-wall (solid line) prediction tends to lie closer to the experimental data than the soft-wall (dashed line) prediction. The hard-wall fit to  $F_\pi(Q^2)$  can be improved for smaller  $Q^2$  by reducing  $1/z_0$  to about 255 MeV, at the expense of the vector meson parameters:  $m_\rho = 613 \text{ MeV}$  and  $f_\rho^{1/2} = 260 \text{ MeV}$ . In the soft-wall model, if one changes the value  $\kappa$  from 388 MeV to 516 MeV in order to fit  $f_\rho$  rather than  $m_\rho$  (which becomes 1032 MeV), the result for  $F_\pi(Q^2)$  lies even further from the experimental data. On the other hand, if one lowers the value for  $\kappa$ , which results in worse predictions for both  $f_\rho$  and  $m_\rho$ , then the fit to  $F_\pi(Q^2)$  lies closer to the experimental data; for example,  $\kappa = 300 \text{ MeV}$  (not plotted) gives the physical  $m_\pi$  and  $f_\pi$  values by taking  $\sigma = (364 \text{ MeV})^3$  and  $m_q = 1.70 \text{ MeV}$ , but then  $m_\rho = 600 \text{ MeV}$  and  $f_\rho^{1/2} = 201 \text{ MeV}$ . Lowering  $\kappa$  to 255 MeV turns out to match  $F_\pi(Q^2)$  data somewhat better, but then  $m_\rho = 510 \text{ MeV}$  and  $f_\rho^{1/2} = 171 \text{ MeV}$ .

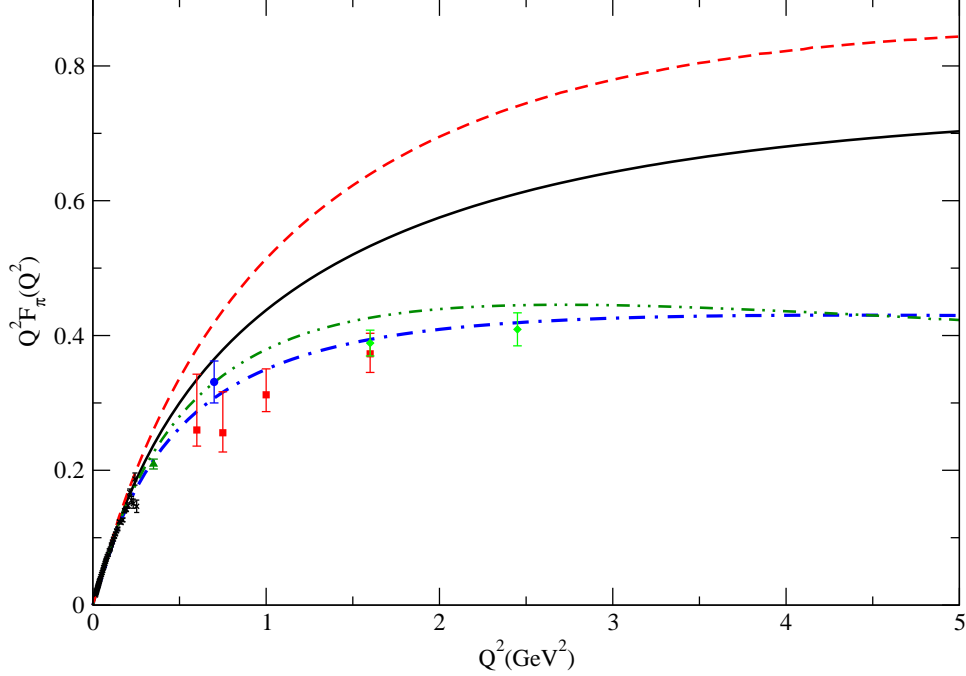


FIG. 2: Spacelike scaling behavior of  $Q^2 F_\pi(Q^2)$  as a function of  $Q^2 = -q^2$ . The symbols are the same as in Fig. 1.

As noted above, once the vector parameters are determined by the value of  $\mu = 1/z_0$  or  $\kappa$ , the pion sector of the models determines best fit values for  $\sigma$  and  $m_q$ . One finds using Eq. (13) that  $f_\pi$  depends mostly on  $\sigma$ , and  $m_\pi$  is then fixed by choosing  $m_q$  to satisfy the GMOR relation. Since, as is apparent in Figs. 1 and 2, the  $F_\pi(Q^2)$  prediction from neither model is particularly good as  $Q^2$  increases, we consider the effect upon  $F_\pi(Q^2)$  of varying  $\sigma$  and  $m_q$  in both models. Empirically, both of the observables scale very close to the square root of the parameters ( $m_\pi^2 \propto m_q$  and  $f_\pi^2 \propto \sigma$ ), but as one might expect,  $F_\pi(Q^2)$  depends much more strongly upon  $\sigma$ . Hence, if one allows  $\sigma$  to float to fit the data for  $F_\pi(Q^2)$ , the precise fit to  $f_\pi$  is spoiled. In particular, lowering the value for  $\sigma$  to  $(254 \text{ MeV})^3$  in the hard-wall model but leaving  $1/z_0 = 322 \text{ MeV}$  gives a much better fit to  $F_\pi(Q^2)$  (dash-dot line in Figs. 1 and 2), but at the price of lowering the prediction of  $f_\pi$  to 64.2 MeV. In the soft-wall model, lowering the value for  $\sigma$  to  $(262 \text{ MeV})^3$  and leaving  $\kappa = 389 \text{ MeV}$  gives a much better fit to  $F_\pi(Q^2)$  (dash-double-dot line in Figs. 1 and 2), but at the price of lowering the prediction of  $f_\pi$  to 52.2 MeV.

Using these form factor results for very low  $Q^2$ , one can extract the pion charge radius  $\langle r_\pi^2 \rangle \equiv -6dF_\pi(Q^2)/dQ^2|_{Q^2=0}$ . The experimental value  $\langle r_\pi^2 \rangle = [0.672(8) \text{ fm}]^2$  [24] lies closer to

the original hard-wall [ $\langle r_\pi^2 \rangle = (0.576 \text{ fm})^2$ ] than the soft-wall [ $\langle r_\pi^2 \rangle = (0.494 \text{ fm})^2$ ] results, as a glance at Fig. 1 suggests. As remarked above, the hard-wall model fits the data better with  $\sigma = (254 \text{ MeV})^3$ , from which one finds  $\langle r_\pi^2 \rangle = (0.645 \text{ fm})^2$ , while setting  $\sigma = (262 \text{ MeV})^3$  for the soft-wall model gives  $\langle r_\pi^2 \rangle = (0.600 \text{ fm})^2$ .

That the soft-wall model gives a shallower prediction for  $F_\pi(Q^2)$ , and hence a smaller value for  $\langle r_\pi^2 \rangle$  compared to the hard-wall prediction, is quite easy to explain numerically. First note that  $V(Q, z)$  in Eqs. (29) and (30) have quite similar  $z$  behaviors, except that  $V(Q, z)$  for the hard wall is cut off at  $z = z_0$ . This fact alone allows for a greater contribution to the integral in Eq. (28) in the soft-wall case. Moreover, the soft wall allows for more penetration of the  $\pi(z)$  and  $\varphi(z)$  fields into the bulk, as verified by our numerical simulations. So together they contribute more to the integration in Eq. (28) and give a higher value of  $F_\pi(Q^2)$  at any particular value of  $Q^2$  than for the hard-wall model.

Finally, we comment upon vector meson dominance and  $F_\pi(q^2)$  in the timelike region. In the hard-wall case we find that  $F_\pi(0)$  is essentially saturated by the first three  $\rho$  meson poles. Explicitly, from the values  $F_n = \gamma_{0,n}/[z_0^2 \sqrt{2}\pi |J_1(\gamma_{0,n})|]$  and  $M_n = \gamma_{0,n}/z_0$ , and using Eq. (33) to compute  $g_{1\pi\pi} = 2.3616$ ,  $g_{2\pi\pi} = -0.8968$ , we find the first few contributions to  $F_\pi(0)$  of  $0.8079 + 0.2830 - 0.0859 = 1.0050$ . However, the convergence is much slower in the soft-wall model. In the soft-wall case one has  $F_n = \kappa^2(\sqrt{2}/\pi)(n+1)^{1/2}$  and  $M_n = 2\kappa(n+1)^{1/2}$ , and computes from Eq. (33) the couplings  $g_{1\pi\pi} = 3.3882$ ,  $g_{2\pi\pi} = 2.9157$ , and  $g_{3\pi\pi} = 2.2946$ . With these values, we find the contributions to  $F_\pi(0)$  of  $0.3751 + 0.2696 + 0.1894 + 0.1291 = 0.9632$ . The next five terms are also positive and bring the sum of pole contributions to 1.138 before turning negative, a pattern that persists for several terms and brings  $F_\pi(0)$  back close to 1. In contrast, results obtained in Refs. [15, 16] for the form factor  $F_\rho(Q^2)$  show very different behavior, requiring fewer resonances for saturation in the soft-wall case.

## V. DISCUSSION AND CONCLUSIONS

In this paper we have considered the problem of pion dynamical properties in holographic QCD, specifically in the context of models for which chiral symmetry breaking, both spontaneous and explicit, is incorporated. In this way it differs from the recent work in Ref. [19], which considers similar problems but contains no parameters analogous to  $\sigma$  and  $m_q$ , and therefore uses a much simpler form for the pion bulk-to-boundary propagator. Nevertheless,

TABLE I: Hard- and soft-wall model predictions for QCD observables, the three model parameters in each case fit to  $m_\pi$ ,  $f_\pi$ , and  $m_\rho$  (indicated by asterisks); all values except  $g_{\rho\pi\pi}$  are in MeV.

Observable	Experiment	Hard-wall	Soft-wall
$m_\pi$	$139.6 \pm 0.0004$ [24]	$139.6^*$	$139.6^*$
$m_\rho$	$775.5 \pm 0.4$ [24]	$775.3^*$	$777.4^*$
$m_{a_1}$	$1230 \pm 40$ [24]	1358	1601
$f_\pi$	$92.4 \pm 0.35$ [24]	$92.1^*$	$87.0^*$
$f_\rho^{1/2}$	$346.2 \pm 1.4$ [25]	329	261
$f_{a_1}^{1/2}$	$433 \pm 13$ [26, 27]	463	558
$g_{\rho\pi\pi}$	$6.03 \pm 0.07$ [24]	4.48	3.33

the basic result that  $F_\pi(Q^2)$  is steeper in the hard-wall than the soft-wall model is common to both calculations.

We also present explicit expressions for the pion bulk-to-boundary propagator  $\partial_z \pi(q, z)$  in all regimes where closed-form analytic solutions are possible. While not directly used in our numerical analysis of  $F_\pi(Q^2)$ , these results are useful for processes involving the tower of  $\pi^{(n)}$  pseudoscalars.

In our numerical studies of  $F_\pi(Q^2)$  we find that the naive hard-wall model appears to be more satisfactory than the soft-wall model over all regions of  $Q^2$ , although the both models can be quantitatively improved by tweaking their parameters (at the expense of fits to other observables). Even before the  $F_\pi(Q^2)$  data is included, one can argue in favor or against either model based upon certain features; the soft-wall model has appropriate linear Regge trajectories but poor agreement for the  $m_\rho^2/f_\rho$  ratio, while the hard-wall model is simpler and has the opposite behavior. The inclusion of the data for  $F_\pi(Q^2)$  suggests an improved model with a semi-hard wall, such as provided by a quasi-“Saxon-Woods” background:

$$e^{-\Phi(z)} = \frac{e^{\lambda^2 z_0^2} - 1}{e^{\lambda^2 z_0^2} + e^{\lambda^2 z^2} - 2}, \quad (34)$$

which has a drop-off at  $z = z_0$  but falls off as  $e^{-\lambda^2 z^2}$  for large  $z$ , thus capturing features of both models and allowing for better predictions. The challenge, as always, is to predict the most observables with the fewest parameters.



## Acknowledgments

We thank Andrei Belitsky and Josh Erlich for valuable discussions. This work was supported by the NSF under Grant No. PHY-0456520.

- 
- [1] J.M. Maldacena, Adv. Theor. Math. Phys. **2**, 231 (1998); [Int. J. Theor. Phys. **38**, 1113 (1999)] [arXiv:hep-th/9711200]; S.S. Gubser, I.R. Klebanov, and A.M. Polyakov, Phys. Lett. B **428**, 105 (1998) [arXiv:hep-th/9802109]; E. Witten, Adv. Theor. Math. Phys. **2**, 253 (1998) [arXiv:hep-th/9802150].
  - [2] J. Polchinski and M.J. Strassler, Phys. Rev. Lett. **88**, 031601 (2002) [arXiv:hep-th/0109174].
  - [3] A. Karch, E. Katz, D.T. Son, and M.A. Stephanov, Phys. Rev. D **74**, 015005 (2006) [arXiv:hep-ph/0602229].
  - [4] J. Erlich, E. Katz, D.T. Son, and M.A. Stephanov, Phys. Rev. Lett. **95**, 261602 (2005) [arXiv:hep-ph/0501128].
  - [5] H. Boschi-Filho and N.R.F. Braga, JHEP **0305**, 009 (2003) [arXiv:hep-th/0212207].
  - [6] G.F. de Teramond and S.J. Brodsky, Phys. Rev. Lett. **94**, 201601 (2005) [arXiv:hep-th/0501022].
  - [7] N. Evans and A. Tedder, Phys. Lett. B **642**, 546 (2006) [arXiv:hep-ph/0609112].
  - [8] D.K. Hong, T. Inami and H.U. Yee, Phys. Lett. B **646**, 165 (2007) [arXiv:hep-ph/0609270].
  - [9] P. Colangelo, F. De Fazio, F. Jugeau and S. Nicotri, Phys. Lett. B **652**, 73 (2007) [arXiv:hep-ph/0703316].
  - [10] H. Forkel, M. Beyer and T. Frederico, JHEP **0707**, 077 (2007) [arXiv:0705.1857 (hep-ph)].
  - [11] L. Da Rold and A. Pomarol, Nucl. Phys. B **721**, 79 (2005) [arXiv:hep-ph/0501218]; JHEP **0601**, 157 (2006) [arXiv:hep-ph/0510268].
  - [12] J. Hirn and V. Sanz, JHEP **0512**, 030 (2005) [arXiv:hep-ph/0507049]; J. Hirn, N. Rius and V. Sanz, Phys. Rev. D **73**, 085005 (2006) [arXiv:hep-ph/0512240].
  - [13] K. Ghoroku, N. Maru, M. Tachibana and M. Yahiro, Phys. Lett. B **633**, 602 (2006) [arXiv:hep-ph/0510334].
  - [14] T. Huang and F. Zuo, arXiv:0708.0936 [hep-ph].
  - [15] H.R. Grigoryan and A.V. Radyushkin, Phys. Lett. B **650**, 421 (2007) [arXiv:hep-ph/0703069].

- [16] H.R. Grigoryan and A.V. Radyushkin, Phys. Rev. D **76**, 095007 (2007) [arXiv:0706.1543 (hep-ph)].
- [17] S. Hong, S. Yoon and M. J. Strassler, JHEP **0604**, 003 (2006) [arXiv:hep-th/0409118].
- [18] A. V. Radyushkin, Phys. Lett. B **642**, 459 (2006) [arXiv:hep-ph/0605116].
- [19] S.J. Brodsky and G.F. de Téramond, arXiv:0707.3859 [hep-ph].
- [20] H.R. Grigoryan and A.V. Radyushkin, Phys. Rev. D **76**, 115007 (2007) [arXiv:0709.0500 (hep-ph)].
- [21] H.J. Kwee and R.F. Lebed, arXiv:0712.1811 [hep-ph].
- [22] M. Abramowitz and I. Stegun, Eds., *Handbook of Mathematical Functions*, Dover, New York (1970).
- [23] Obtaining this form requires the use of the vector field equation of motion, Eq. (5). We thank Josh Erlich for pointing this out.
- [24] S. Eidelman *et al.* (PDG), Phys. Lett. B **592**, 1 (2004).
- [25] J. F. Donoghue, E. Golowich, and B. R. Holstein, *Dynamics of the Standard Model* (Cambridge University Press, Cambridge 1992)
- [26] D. T. Son and M. A. Stephanov, Phys. Rev. D **69**, 065020 (2004).
- [27] N. Isgur, C. Morningstar, and C. Reader, Phys. Rev. D **39**, 1357 (1989).
- [28] S.R. Amendolia *et al.*, Phys. Lett. **B138**, 454 (1984); Nucl. Phys. **B277**, 168 (1986).
- [29] P. Brauel *et al.*, Phys. Lett. **B69**, 253 (1977); P. Brauel *et al.*, Z. Phys. **C3**, 101 (1979).
- [30] H. Ackermann *et al.*, Nucl. Phys. **B137**, 294 (1978).
- [31] V. Tadevosyan *et al.* [Jefferson Lab F(pi) Collaboration], Phys. Rev. C **75**, 055205 (2007) [arXiv:nucl-ex/0607007].
- [32] T. Horn *et al.* [Fpi2 Collaboration], Phys. Rev. Lett. **97**, 192001 (2006) [arXiv:nucl-ex/0607005].
- [33] C.J. Bebek *et al.*, Phys. Rev. D **17**, 1693 (1978).